Received 10 August 2008
Accepted 15 December 2008

Simulation of soliton-like waves generated by topography with conservative fully discrete shallow-water arbitrary-order schemes

Yuri N. Skiba
Centro de Ciencias de la Atmósfera (CCA), Universidad Nacional Autónoma de México (UNAM), México City, México, and
Denis M. Filatov
Centro de Investigación en Computación (CIC), Instituto Politécnico Nacional (IPN), México City, México

Abstract

Purpose – The purpose of this paper is to suggest a new approach to the numerical simulation of shallow-water flows both in plane domains and on the sphere.

Design/methodology/approach – The approach involves the technique of splitting of the model operator by geometric coordinates and by physical processes. Specially chosen temporal and spatial approximations result in one-dimensional finite difference schemes that conserve the mass and the total energy. Therefore, the mass and the total energy of the whole two-dimensional split scheme are kept constant too.

Findings – Explicit expressions for the schemes of arbitrary approximation orders in space are given. The schemes are shown to be mass- and energy-conserving, and hence absolutely stable because the square root of the total energy is the norm of the solution. The schemes of the first four approximation orders are then tested by simulating nonlinear solitary waves generated by a model topography. In the analysis, the primary attention is given to the study of the time-space structure of the numerical solutions.

Originality/value – The approach can be used for the numerical simulation of shallow-water flows in domains of both Cartesian and spherical geometries, providing the solution adequate from the physical and mathematical standpoints in the sense of keeping its mass and total energy constant even when fully discrete shallow-water models are applied.

Keywords Difference equations, Finite difference methods, Waves, Topography, Simulation, Numerical analysis

Paper type Research paper

1. Introduction

Consider the shallow-water equations (SWEs) written in the divergent form (Samarskii and Popov, 1969; Shokin, 1988; Skiba, 1995):

$$\frac{\partial U}{\partial t}+\frac{1}{2}\left(\frac{\partial uU}{\partial x}+u\frac{\partial U}{\partial x}\right)+\frac{1}{2}\left(\frac{\partial vU}{\partial y}+v\frac{\partial U}{\partial y}\right)-fV=-gz\frac{\partial h}{\partial x}, \tag{1}$$

$$\frac{\partial V}{\partial t}+\frac{1}{2}\left(\frac{\partial uV}{\partial x}+u\frac{\partial V}{\partial x}\right)+\frac{1}{2}\left(\frac{\partial vV}{\partial y}+v\frac{\partial V}{\partial y}\right)+fU=-gz\frac{\partial h}{\partial y}, \tag{2}$$

$$\frac{\partial H}{\partial t}+\frac{\partial zU}{\partial x}+\frac{\partial zV}{\partial y}=0. \tag{3}$$

International Journal of Numerical Methods for Heat & Fluid Flow
Vol. 19 No. 8, 2009
pp. 982-1007

0961-5539
DOI 10.1108/09615530910994469

Here $z := \sqrt{H}, U := zu$ and $V := zv, (u(x,y,t), v(x,y,t))^{\mathrm{T}}$ is the fluid's velocity field, $H = H(x,y,t)$ is the fluid's depth (or, in meteorological problems, the atmospheric column's height), $f = f(y)$ is the Coriolis acceleration, $h = h(x,y,t)$ is the free surface height and $h_r = h - H$ is the underlying relief's height. We consider the problem subject to appropriate initial conditions and the periodic boundary conditions in x and y in a doubly periodic domain D.

System (1)-(3) possesses the mass, energy and potential enstrophy conservation laws (Pedlosky, 1982; Vreugdenhil, 1994):

$$\frac{\partial M(t)}{\partial t} \equiv \frac{\partial}{\partial t}\int_D H dxdy = 0, \tag{4}$$

$$\frac{\partial E(t)}{\partial t} \equiv \frac{\partial}{\partial t}\int_D \left(\frac{U^2+V^2}{2} + \frac{gh^2}{2}\right) dxdy = 0, \tag{5}$$

$$\frac{\partial J(t)}{\partial t} \equiv \frac{\partial}{\partial t}\int_D \frac{(\partial v/\partial x - \partial u/\partial y + f)^2}{2H} dxdy = 0, \tag{6}$$

which establish specific limitations on the shallow-water equations (SWM) solution, or, in other words, on the motion of the fluid. However, in a fully discrete (i.e. discrete both in space and in time) SWMs the total energy and the potential enstrophy usually stop being invariant (Vreugdenhil, 1994). This leads to the numerical instability and the false energy distribution over the spectrum of movements of different scales (Morton and Mayers, 1994), and as a consequence, the numerical results, especially at long-term calculations, can be far from the exact ones in some norms (note that the square root of the total energy is the most natural norm for the SWM). In order to reduce the approximation errors and eliminate numerical instability, conservative schemes have to be employed (Samarskii and Popov, 1969; Shokin, 1988). Moreover, for obtaining physically reliable numerical results and avoiding numerical instability effects finite difference schemes should conserve as many shallow-water invariants of motion as possible (Williamson, 1979).

In the last three decades there have been developed several approaches for constructing semidiscrete (discrete in space, but continuous in time) models that conserve some or other invariants of motion of the SWEs. However, all such models stop being conservative when the time derivatives are discretised by using an explicit approximation (Arakawa and Lamb, 1981; Kim, 1984; Ringler and Randall, 2002; Sadourny, 1975; Salmon, 2004; Takano and Wurtele, 1982). Yet, even if the Crank-Nicolson approximation is used to keep the scheme conservative, the existing methods possess certain disadvantages. This is especially true for high-order schemes where either complicated spatial grids are utilised (Ringler and Randall, 2002) or rather sophisticated finite difference stencils are employed (Salmon, 2004). Specifically, the use of multipointed complex stencils or geodesic grids restricts the applicability of the corresponding schemes. For instance, the scheme developed in Salmon, (2004), because of the complexity of the spatial stencil, is applicable only in the Cartesian geometry with periodic boundary conditions in both directions, and it cannot be used on a sphere nor on the plane in nonperiodic bounded domains.

Recently a new approach to the numerical simulation of shallow-water flows has been suggested both in plane domains (Skiba, 1995) and on the sphere (Skiba and Filatov, 2007, 2008). The approach permits conserving the mass and the total energy of the system when it is fully discretised, i.e. both in time and in space. Yet, it provides

substantial benefits in the computational cost of solution and, as applied to a doubly periodic manifold, allows to construct conservative finite difference schemes of arbitrary approximation orders in space. Moreover, if the SWM is considered on the entire sphere (which is *not* a doubly periodic manifold) then the method permits to use the same numerical algorithms as for a doubly periodic region. Thereby, for the spherical SWM conservative arbitrary order finite differences. Schemes can also be constructed. The approach involves the technique of splitting of the model operator by geometric coordinates and by physical processes (Marchuk, 1982; Skiba, 1995). Specially chosen temporal and spatial approximations result in one-dimensional schemes that conserve the mass and the total energy, and so the mass and the total energy of the whole two-dimensional split scheme are kept constant too. In fact, an infinite set of such schemes is suggested. The schemes are either linear or nonlinear depending on the choice of certain parameters.

In this work conservative fully discrete splitting-based schemes for the shallow-water flows on the whole sphere are considered in detail. We give explicit expressions for the schemes of arbitrary approximation orders in space. The schemes are shown to be mass- and energy-conserving, and hence are absolutely stable because the square root of the total energy is the norm of the solution. The schemes of the first four approximation orders are then tested by simulating nonlinear solitary waves generated by a model topography.

The paper is organised as follows. In section 2 we begin from the demonstration of benefits we gain having written the SWEs in the divergent form. There we also employ the Crank-Nicolson approximation. Independently, in section 3 we use operator splitting and introduce three simpler one-dimensional subproblem. Joining all together, in section 4 we construct different order finite difference schemes for the SWM studied on a doubly periodic manifold. We shall explicitly write the schemes of the first four orders, as well as introduce a general formula for an arbitrary-order scheme. Section 5 extends the "planar" approach to the case of spherical geometry. In section 6 we test the developed numerical method by simulating nonlinear soliton-like waves generated by a model topography. The time-space structure of the solution is analysed in detail and the temporal behaviour of the potential enstrophy is studied. In section 7 we make a concluding summary.

2. Divergent form of the SWEs and Crank-Nicolson approximation

The form of system (1)-(3) is called "divergent" for the following reasons.

First, the sum of the last two terms of equation (3) represents the divergence of the vector $(zU, zV)^{\mathrm{T}}$. So, integration of (3) over D, given the periodic boundary conditions, eliminates the divergent terms that yields the mass conservation law (4). Second, equations (1)-(2) contain the terms $\partial aB/\partial r + a(\partial B/\partial r)$, where $a = \{u, v\}, B = \{U, V\}$ and $r = \{x, y\}$, which, being multiplied by B, take the divergent form $\partial aB^2/\partial r$. For example, for the first equation we obtain $[(\partial uU/\partial x + u(\partial U/\partial x)) + (\partial vU/\partial y + v(\partial U/\partial y))]U = \partial uU^2/\partial x + \partial vU^2/\partial y = \nabla \cdot (uU^2, vU^2)^{\mathrm{T}} \equiv \mathrm{div}(uU^2, vU^2)^{\mathrm{T}}$. Integration over the domain D, given the periodic boundary conditions, also eliminates the divergent terms. Further, sum of the terms $gz(\partial h/\partial r)$ and $\partial zB/\partial r$, multiplied by B and gh, respectively, also takes the divergent form $\partial gzBh/\partial r$ and thus vanishes when integrating over D. This leads to the total (kinetic plus potential) energy conservation law (5).

The "divergence" property of system (1)-(3) is the crucial point. Specifically, it can be shown that certain discrete approximations of the "divergent" terms, given the periodicity of D in both directions, vanish when summing over all the grid nodes. For

instance, taking the approximation:

$$\frac{\partial uU}{\partial x} + u\frac{\partial U}{\partial x} \approx \frac{u_{kl}U_{kl} - u_{k-1,l}U_{k-1,l}}{\Delta x} + u_{kl}\frac{U_{k+1,l} - U_{kl}}{\Delta x} =: R_{kl}, \tag{7}$$

we easily obtain:

$$\sum_{k,l} R_{kl}U_{kl} = \cdots = 0. \tag{8}$$

As to the Coriolis terms, the sum of the terms $-fV$ and fU, being multiplied by U and V, respectively, simply disappears. Consequently, the problem of construction of mass- and energy-conserving finite difference schemes reduces to the search for such appropriate approximations of the divergent terms of (1)-(3) that the operator of the corresponding discrete SWM would be antisymmetric, as the original SWM operator is.

The only temporal approximation that keeps antisymmetricity for a finite difference operator is the Crank-Nicolson scheme. Indeed, consider the differential problem:

$$\frac{\partial \vec{\eta}}{\partial t} + L\vec{\eta} = 0, \tag{9}$$

$$\vec{\eta}|_{t=0} = \vec{g}(\mathbf{x}) \tag{10}$$

with an antisymmetric operator L, and a family of finite difference schemes:

$$\frac{\vec{\eta}^{n+1} - \vec{\eta}^{n}}{\tau} + L\left(\sigma\vec{\eta}^{n} + (1-\sigma)\vec{\eta}^{n+1}\right) = 0, \qquad 0 \le \sigma \le 1, \tag{11}$$

$$\vec{\eta}^{0} = \vec{g}(\mathbf{x}). \tag{12}$$

The antisymmetry means that:

$$\langle L\vec{\gamma}, \vec{\gamma}\rangle = 0 \qquad \forall\vec{\gamma} \neq 0,$$

where $\langle\cdot,\cdot\rangle$ is a scalar product. Multiplying (11) by $\sigma\vec{\eta}^{n} + (1-\sigma)\vec{\eta}^{n+1}$ and integrating, we obtain:

$$\frac{1}{\tau}\left\langle \vec{\eta}^{n+1} - \vec{\eta}^{n}, \sigma\vec{\eta}^{n} + (1-\sigma)\vec{\eta}^{n+1}\right\rangle = 0,$$

and hence the norm of the solution keeps constant only when $\sigma = \frac{1}{2}$, which corresponds to the Crank-Nicolson approximation (Marchuk, 1982; Yanenko, 1971).

These properties of the divergent form of system (1)-(3) will essentially be used in section 4 for the construction of conservative finite difference schemes.

3. Operator splitting

In each small time interval we split system (1)-(3) into three simpler subproblems. First, fixing the coordinate y, in the direction x we get:

$$\frac{\partial U}{\partial t} + \frac{1}{2}\left(\frac{\partial uU}{\partial x} + u\frac{\partial U}{\partial x}\right) = -gz\frac{\partial h}{\partial x}, \tag{13}$$

$$\frac{\partial V}{\partial t}+\frac{1}{2}\left(\frac{\partial uV}{\partial x}+u\frac{\partial V}{\partial x}\right)=0, \tag{14}$$

$$\frac{\partial H}{\partial t}+\frac{\partial zU}{\partial x}=0. \tag{15}$$

Second, fixing x, in the direction y we obtain:

$$\frac{\partial U}{\partial t}+\frac{1}{2}\left(\frac{\partial vU}{\partial y}+v\frac{\partial U}{\partial y}\right)=0, \tag{16}$$

$$\frac{\partial V}{\partial t}+\frac{1}{2}\left(\frac{\partial vV}{\partial y}+v\frac{\partial V}{\partial y}\right)=-gz\frac{\partial h}{\partial y}, \tag{17}$$

$$\frac{\partial H}{\partial t}+\frac{\partial zV}{\partial y}=0. \tag{18}$$

Finally, for the rotation process we write:

$$\frac{\partial U}{\partial t}-fV=0, \tag{19}$$

$$\frac{\partial V}{\partial t}+fU=0. \tag{20}$$

Equations (13)-(15) and (16)-(18) represent one-dimensional PDE systems, while equations (19)-(20) form a system of ordinary differential equations. Note that each split system conserves the mass and the total energy.

It is important to remark that for an arbitrary boundary value problem one has to be careful while using the method of splitting. The crucial point here is the splitting of boundary conditions, because the latter must be split in such a way that (1) all the split subproblems be well-posed and (2) in each small time interval, the solution obtained after resolving all the split subproblems converge to the solution to the original unsplit problem. Several examples on this topic can be found in D'yakonov (1964, 1972). However, since we consider problem (1)-(3) in a doubly periodic domain, both of these requirements are satisfied (Marchuk, 1982).

4. Conservative finite difference schemes

Taking into account the results of sections 2 and 3, we shall now approximate each split system by the Crank-Nicolson scheme in time. On the other hand, since the only restriction on *spatial* approximations is that the resulting "divergent" terms must disappear while summing over all the grid nodes, different order finite difference stencils can be involved for constructing *arbitrary* order conservative schemes in space. Yet, the functions u, v and z can be approximated in an absolutely arbitrary manner, which will allow to develop useful filters for reducing computational modes in the numerical solution in case of using central spatial finite differences stencils (Skiba and Filatov, 2007, 2008).

So, let: $\tau = t_{n+1} - t_n, \Delta x = x_{k+1} - x_k, \Delta y = y_{l+1} - y_l, f_l = f(y_l), W_{kl}^n = W(x_k, y_l, t_n)$ and

$$W_{kl} = \frac{W_{kl}^{n+1} + W_{kl}^n}{2}, \tag{21}$$

where the symbol W represents any of the functions u, v, H, h, U, V, z.

First-order schemes. Consider a small time interval (t_n, t_{n+1}). We discretise (13)-(15) in the form (the index l in the y-direction is omitted in order not to complicate the formulas):

$$\frac{U_k^{n+1} - U_k^n}{\tau} + \frac{1}{2}\left(\frac{\overline{u}_k U_{k+1} - \overline{u}_{k-1} U_{k-1}}{\Delta x}\right) = -g\overline{z}_k \frac{h_{k+1} - h_k}{\Delta x}, \tag{22}$$

$$\frac{V_k^{n+1} - V_k^n}{\tau} + \frac{1}{2}\left(\frac{\overline{u}_k V_{k+1} - \overline{u}_{k-1} V_{k-1}}{\Delta x}\right) = 0, \tag{23}$$

$$\frac{H_k^{n+1} - H_k^n}{\tau} + \frac{\overline{z}_k U_k - \overline{z}_{k-1} U_{k-1}}{\Delta x} = 0. \tag{24}$$

Here we used the first-order approximation $\partial uB/\partial x + u(\partial B/\partial x) \approx u_k B_k - u_{k-1} B_{k-1}/\Delta x + u_k(B_{k+1} - B_k/\Delta x) = u_k B_{k+1} - u_{k-1} B_{k-1}/\Delta x$. Another first-order scheme can be obtained if $\partial uB/\partial x + u(\partial B/\partial x) \approx u_{k+1} B_{k+1} - u_k B_k/\Delta x + u_k(B_k - B_{k-1})/\Delta x = u_{k+1} B_{k+1} - u_k B_{k-1}/\Delta x$; so:

$$\frac{U_k^{n+1} - U_k^n}{\tau} + \frac{1}{2}\left(\frac{\overline{u}_{k+1} U_{k+1} - \overline{u}_k U_{k-1}}{\Delta x}\right) = -g\overline{z}_k \frac{h_k - h_{k-1}}{\Delta x}, \tag{25}$$

$$\frac{V_k^{n+1} - V_k^n}{\tau} + \frac{1}{2}\left(\frac{\overline{u}_{k+1} V_{k+1} - \overline{u}_k V_{k-1}}{\Delta x}\right) = 0, \tag{26}$$

$$\frac{H_k^{n+1} - H_k^n}{\tau} + \frac{\overline{z}_{k+1} U_{k+1} - \overline{z}_k U_k}{\Delta x} = 0. \tag{27}$$

Second-order scheme. If we employ the central second-order finite difference stencil then we shall have the scheme:

$$\begin{aligned} &\frac{U_k^{n+1} - U_k^n}{\tau} + \frac{1}{2}\left(\frac{\overline{u}_{k+1} U_{k+1} - \overline{u}_{k-1} U_{k-1}}{2\Delta x} + \overline{u}_k \frac{U_{k+1} - U_{k-1}}{2\Delta x}\right) \\ &\quad = -g\overline{z}_k \frac{h_{k+1} - h_{k-1}}{2\Delta x} \end{aligned} \tag{28}$$

$$\frac{V_k^{n+1}-V_k^n}{\tau}+\frac{1}{2}\left(\frac{\overline{u}_{k+1}V_{k+1}-\overline{u}_{k-1}V_{k-1}}{2\Delta x}+\overline{u}_k\frac{V_{k+1}-V_{k-1}}{2\Delta x}\right)=0, \tag{29}$$

$$\frac{H_k^{n+1}-H_k^n}{\tau}+\frac{\overline{z}_{k+1}U_{k+1}-\overline{z}_{k-1}U_{k-1}}{2\Delta x}=0. \tag{30}$$

Third-order schemes. Increasing the approximation order to three, we can write either:

$$\begin{aligned}\frac{\partial aB}{\partial x}+a\frac{\partial B}{\partial x}&\approx\frac{11a_kB_k-18a_{k-1}B_{k-1}+9a_{k-2}B_{k-2}-2a_{k-3}B_{k-3}}{6\Delta x}\\&\quad+a_k\frac{2B_{k+3}-9B_{k+2}+18B_{k+1}-11B_k}{6\Delta x}\\&=a_k\frac{2B_{k+3}-9B_{k+2}+18B_{k+1}}{6\Delta x}\\&\quad+\frac{-18a_{k-1}B_{k-1}+9a_{k-2}B_{k-2}-2a_{k-3}B_{k-3}}{6\Delta x}=:A^{(3)}_{-+}(a,B)\end{aligned} \tag{31}$$

or,

$$\begin{aligned}\frac{\partial aB}{\partial x}+a\frac{\partial B}{\partial x}&\approx\frac{2a_{k+3}B_{k+3}-9a_{k+2}B_{k+2}+18a_{k+1}B_{k+1}-11a_kB_k}{6\Delta x}\\&\quad+a_k\frac{11B_k-18B_{k-1}+9B_{k-2}-2B_{k-3}}{6\Delta x}\\&=\frac{18a_{k+1}B_{k+1}-9a_{k+2}B_{k+2}+2a_{k+3}B_{k+3}}{6\Delta x}\\&\quad+a_k\frac{-18B_{k-1}+9B_{k-2}-2B_{k-3}}{6\Delta x}=:A^{(3)}_{+-}(a,B),\end{aligned} \tag{32}$$

which will provide either with:

$$\frac{U_k^{n+1}-U_k^n}{\tau}+\frac{1}{2}A^{(3)}_{-+}(\overline{u},U)=-g\overline{z}_k\frac{2h_{k+3}-9h_{k+2}+18h_{k+1}-11h_k}{6\Delta x}, \tag{33}$$

$$\frac{V_k^{n+1}-V_k^n}{\tau}+\frac{1}{2}A^{(3)}_{-+}(\overline{u},V)=0, \tag{34}$$

$$\frac{H_k^{n+1}-H_k^n}{\tau}+\frac{11\overline{z}_kU_k-18\overline{z}_{k-1}U_{k-1}+9\overline{z}_{k-2}U_{k-2}-2\overline{z}_{k-3}U_{k-3}}{6\Delta x}=0 \tag{35}$$

or with,

$$\frac{U_k^{n+1}-U_k^n}{\tau}+\frac{1}{2}A^{(3)}_{+-}(\overline{u},U)=-g\overline{z}_k\frac{11h_k-18h_{k-1}+9h_{k-2}-2h_{k-3}}{6\Delta x}, \tag{36}$$

$$\frac{V_k^{n+1} - V_k^n}{\tau} + \frac{1}{2} A_{+-}^{(3)}(\overline{u}, V) = 0, \tag{37}$$

$$\frac{H_k^{n+1} - H_k^n}{\tau} + \frac{2\overline{z}_{k+3}U_{k+3} - 9\overline{z}_{k+2}U_{k+2} + 18\overline{z}_{k+1}U_{k+1} - 11\overline{z}_k U_k}{6\Delta x} = 0, \tag{38}$$

respectively.

Fourth-order scheme. With the central fourth-order stencil we shall obtain the scheme:

$$\frac{U_k^{n+1} - U_k^n}{\tau} + \frac{1}{2}\left(\frac{-\overline{u}_{k+2}U_{k+2} + 8\overline{u}_{k+1}U_{k+1} - 8\overline{u}_{k-1}U_{k-1} + \overline{u}_{k-2}U_{k-2}}{12\Delta x} + \overline{u}_k \frac{-U_{k+2} + 8U_{k+1} - 8U_{k-1} + U_{k-2}}{12\Delta x}\right) = -g\overline{z}_k \frac{-h_{k+2} + 8h_{k+1} - 8h_{k-1} + h_{k-2}}{12\Delta x}, \tag{39}$$

$$\frac{V_k^{n+1} - V_k^n}{\tau} + \frac{1}{2}\left(\frac{-\overline{u}_{k+2}V_{k+2} + 8\overline{u}_{k+1}V_{k+1} - 8\overline{u}_{k-1}V_{k-1} + \overline{u}_{k-2}V_{k-2}}{12\Delta x} + \overline{u}_k \frac{-V_{k+2} + 8V_{k+1} - 8V_{k-1} + V_{k-2}}{12\Delta x}\right) = 0, \tag{40}$$

$$\frac{H_k^{n+1} - H_k^n}{\tau} + \frac{-\overline{z}_{k+2}U_{k+2} + 8\overline{z}_{k+1}U_{k+1} - 8\overline{z}_{k-1}U_{k-1} + \overline{z}_{k-2}U_{k-2}}{12\Delta x} = 0, \tag{41}$$

and so on.

Arbitrary-order schemes Generally, an arbitrary p-order noncentral finite difference scheme can be obtained either with (backward-forward approximation):

$$\frac{\partial aB}{\partial r} + a\frac{\partial B}{\partial r} \approx \frac{1}{\Delta r}\sum_{i=0}^{p} c_{k-i}(\overline{a}B)_{k-i} - \overline{a}_k \frac{1}{\Delta r}\sum_{i=0}^{p} c_{k-i}B_{k+i}, \tag{42}$$

$$z\frac{\partial h}{\partial r} \approx -z_k \frac{1}{\Delta r}\sum_{i=0}^{p} c_{k-i}h_{k+i}, \tag{43}$$

$$\frac{\partial zB}{\partial r} \approx \frac{1}{\Delta r}\sum_{i=0}^{p} c_{k-i}(\overline{z}B)_{k-i} \tag{44}$$

or with (forward-backward approximation):

$$\frac{\partial aB}{\partial r} + a\frac{\partial B}{\partial r} \approx -\frac{1}{\Delta r}\sum_{i=0}^{p} c_{k-i}(\overline{a}B)_{k+i} + \overline{a}_k \frac{1}{\Delta r}\sum_{i=0}^{p} c_{k-i}B_{k-i}, \tag{45}$$

$$z\frac{\partial h}{\partial r} \approx z_k \frac{1}{\Delta r}\sum_{i=0}^{p} c_{k-i}h_{k-i}, \tag{46}$$

$$\frac{\partial zB}{\partial r} \approx -\frac{1}{\Delta r}\sum_{i=0}^{p} c_{k-i}(\overline{z}B)_{k+i}. \tag{47}$$

An arbitrary q-even-order central finite difference scheme comes from:

$$\frac{\partial aB}{\partial r} + a\frac{\partial B}{\partial r} \approx \frac{1}{\Delta r}\sum_{i=-\frac{q}{2}}^{\frac{q}{2}} \hat{c}_{k+i}(aB)_{k+i} + a_k \frac{1}{\Delta r}\sum_{i=-\frac{q}{2}}^{\frac{q}{2}} \hat{c}_{k+i}B_{k+i}, \tag{48}$$

$$z\frac{\partial h}{\partial r} \approx z_k \frac{1}{\Delta r}\sum_{i=-\frac{q}{2}}^{\frac{q}{2}} \hat{c}_{k+i}h_{k+i}, \tag{49}$$

$$\frac{\partial zB}{\partial r} \approx \frac{1}{\Delta r}\sum_{i=-\frac{q}{2}}^{\frac{q}{2}} \hat{c}_{k+i}(zB)_{k+i}. \tag{50}$$

The coefficients $\{c_i\}$ and $\{\hat{c}_i\}$ determine the corresponding finite difference stencils and can be found e.g. in Korn and Korn (1968). For example, for scheme (28) we have $q = 2$ and $\hat{c}_{k+1} = -\hat{c}_{k-1} = \frac{1}{2}$, $\hat{c}_k = 0$.

Similarly one can write down arbitrary-order finite difference schemes in the y-direction (subproblem (16)-(18)).

As to the rotational process (equations (19)-(20)), we have:

$$\frac{U_{kl}^{n+1} - U_{kl}^{n}}{\tau} - f_l V_{kl} = 0, \tag{51}$$

$$\frac{V_{kl}^{n+1} - V_{kl}^{n}}{\tau} + f_l U_{kl} = 0. \tag{52}$$

Since we discretised the spatial derivatives $\partial\{U, V, h\}/\partial\{x, y\}$ using (21) and because all the split difference operators are antisymmetric, each of the developed schemes conserves the mass and total energy. As a result, the mass and total energy of the whole discrete model (consisting of the three split models) are conserved too.

It is important that all the schemes coming from (42)-(44), (45)-(47) or (48)-(50) can be resolved by a direct (i.e. non-iterative) method, and therefore the conservation laws are

not violated. Indeed, consider, for example, equation (22). For its right-hand side, taking into account (21), we can write $-g\bar{z}_k(h_{k+1}-h_k/\Delta x) = -g\bar{z}_k(h_{k+1}^{n+1}+h_{k+1}^n-h_k^{n+1}-h_k^n)/2\Delta x$, and hence, expressing from (24) the function H_k^{n+1} and then substituting $h_k^{n+1} = H_k^{n+1} + h_{rk}$ into (22), we shall obtain:

$$\frac{U_k^{n+1}-U_k^n}{\tau} + P_1 + P_2 = P_3 + P_4, \tag{53}$$

where,

$$P_1 = \frac{1}{4\Delta x}S_1(n+1), \quad P_2 = -\frac{g\bar{z}_k\tau}{4\Delta x^2}S_2(n+1),$$
$$P_3 = -\frac{1}{4\Delta x}S_1(n), \quad P_4 = -\frac{g\bar{z}_k}{2\Delta x}\left(2(h_{k+1}^n-h_k^n) - \frac{\tau}{2\Delta x}S_2(n)\right),$$
$$S_1(n) = \overline{u}_k U_{k+1}^n - \overline{u}_{k-1}U_{k-1}^n, \quad S_2(n) = \bar{z}_{k+1}U_{k+1}^n - 2\bar{z}_k U_k^n + \bar{z}_{k-1}U_{k-1}^n.$$

Therefore, if we define:

$$\overline{u}_{kl} = u_{kl}^n, \qquad \overline{v}_{kl} = v_{kl}^n, \qquad \bar{z}_{kl} = z_{kl}^n, \tag{54}$$

then scheme (53), (23)-(24) can be solved by a direct linear algebra method. Of course, if (54) holds then all the other schemes in x and in y also reduce to systems of linear algebraic equations. Moreover, due to the use of splitting all these systems will have M-diagonal matrices, and thus band linear solvers can be employed for their solution (Press *et al.*, 1992).

Scheme (51)-(52) is independent of the choice of the functions $\overline{u}_{kl}$, $\overline{v}_{kl}$ and $\bar{z}_{kl}$, and hence it can be transformed to the form:

$$U_{kl}^{n+1} = \frac{\left(1-\frac{\tau^2}{4}f_l^2\right)U_{kl}^n + \tau f_l V_{kl}^n}{1+\frac{\tau^2}{4}f_l^2}, \tag{55}$$

$$V_{kl}^{n+1} = \frac{\left(1-\frac{\tau^2}{4}f_l^2\right)V_{kl}^n - \tau f_l U_{kl}^n}{1+\frac{\tau^2}{4}f_l^2}. \tag{56}$$

As we noted in section 3, the functions $\overline{u}_{kl}$, $\overline{v}_{kl}$ and $\bar{z}_{kl}$ can be defined in an arbitrary way.

So, apart from (54) we can write:

$$\overline{w}_{kl} = \sum_{i,j}\alpha_{k+i,l+j}^{(w)} w_{k+i,l+j}^n, \qquad w = \{u, v, z\}, \tag{57}$$

where $\alpha_{k+i,l+j}^{(w)}$ are weight coefficients for u, v and z, while i, j vary in some ranges over neighbouring nodes. Such approximations may be useful for reducing computational modes of the solutions if one employs an even-order central finite difference scheme. Another possible choice could be $\overline{u}_{kl} = u_{kl}$, $\overline{v}_{kl} = v_{kl}$ and $\bar{z}_{kl} = z_{kl}$. However, in this case all the subsequent schemes in x and in y will be nonlinear (Skiba, 1995; Skiba and Filatov, 2007) and an iterative procedure must be used for their solution, which will not keep the invariants of motion constant.

5. Shallow-water schemes on the sphere

The sphere is a very important geometric manifold for many meteorological applications of the SWEs. A great advantage of the splitting-based approach is that it allows using the developed "planar" algorithm for studying shallow-water flows on a rotating sphere.

Consider the SWEs in the spherical coordinates (λ, φ):

$$\frac{\partial U}{\partial t} + \frac{1}{R\cos\varphi}\left[\frac{1}{2}\left(\frac{\partial uU}{\partial \lambda} + u\frac{\partial U}{\partial \lambda}\right) + \frac{1}{2}\left(\frac{\partial vU\cos\varphi}{\partial \varphi} + v\cos\varphi\frac{\partial U}{\partial \varphi}\right)\right] - \left(f + \frac{u}{R}\tan\varphi\right)V = -\frac{gz}{R\cos\varphi}\frac{\partial h}{\partial \lambda}, \tag{58}$$

$$\frac{\partial V}{\partial t} + \frac{1}{R\cos\varphi}\left[\frac{1}{2}\left(\frac{\partial uV}{\partial \lambda} + u\frac{\partial V}{\partial \lambda}\right) + \frac{1}{2}\left(\frac{\partial vV\cos\varphi}{\partial \varphi} + v\cos\varphi\frac{\partial V}{\partial \varphi}\right)\right] + \left(f + \frac{u}{R}\tan\varphi\right)U = -\frac{gz}{R}\frac{\partial h}{\partial \varphi}, \tag{59}$$

$$\frac{\partial H}{\partial t} + \frac{1}{R\cos\varphi}\left[\frac{\partial zU}{\partial \lambda} + \frac{\partial zV\cos\varphi}{\partial \varphi}\right] = 0. \tag{60}$$

Here λ is the longitude (positive eastward), φ is the latitude (positive northward), R is the sphere's radius, $f = 2\Omega\sin\varphi$ and Ω is the angular rotation rate. Problem (58)-(60) is being studied on the sphere S.

The grid on the sphere is taken as follows:

$$S_{\Delta\lambda,\Delta\varphi} = \left\{(\lambda_k, \varphi_l) : \tfrac{\Delta\lambda}{2} \le \lambda_k < 2\pi + \tfrac{\Delta\lambda}{2}, -\tfrac{\pi}{2} + \tfrac{\Delta\varphi}{2} \le \varphi_l \le \tfrac{\pi}{2} - \tfrac{\Delta\varphi}{2}\right\}. \tag{61}$$

Note that in (61) we moved the grid to a half step in the direction φ: $\{\varphi_l\}_{1/2}^{L-1/2} = \{-\frac{\pi}{2} + \frac{\Delta\varphi}{2} + l\Delta\varphi, l = \overline{0, L-1}\}$, because due to the metric term $1/R\cos\varphi$ equations (58)-(60) are not valid in the poles. Therefore we do cover the whole sphere, and at the same time do not have to find the solution at the pole nodes (Williamson, 1979). This grid is used for computing the solution in the $\lambda-$direction (Figure 1).

The point of using the operator splitting in the spherical geometry is that although the sphere is evidently *not* a doubly periodic manifold, our algorithm developed for a doubly periodic domain can be applied to the sphere too. Indeed, for computing the solution in the $\varphi-$direction we can represent the same grid in the other manner (Figure 2):

$$S_{\Delta\lambda,\Delta\varphi} = \left\{(\lambda_k, \varphi_l) : \tfrac{\Delta\lambda}{2} \le \lambda_k \le \pi - \tfrac{\Delta\lambda}{2}, \tfrac{\Delta\varphi}{2} \le \varphi_l < 2\pi + \tfrac{\Delta\varphi}{2}\right\}. \tag{62}$$

One can see that the grid covering (62) has the same nodes as in (61). Thus, after making slight modifications in (42)-(44), (45)-(47) and (48)-(50) (in fact, merely the metric term $1/R\cos\varphi$ has to be added, as well) those formulas can be applied for constructing conservative finite difference schemes for system (58)-(60). For instance, the second-order finite difference scheme in the direction λ has the form:

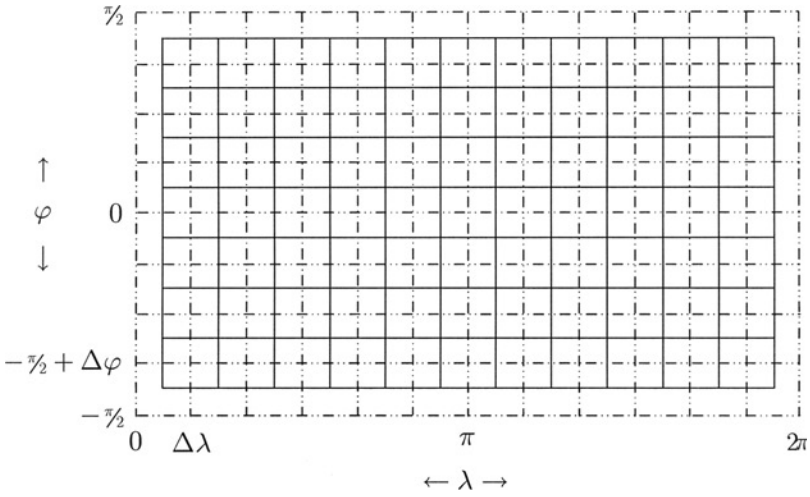

Figure 1.
The first coordinate map (dash-dot lines) and the corresponding grid covering (solid lines) for the sphere S

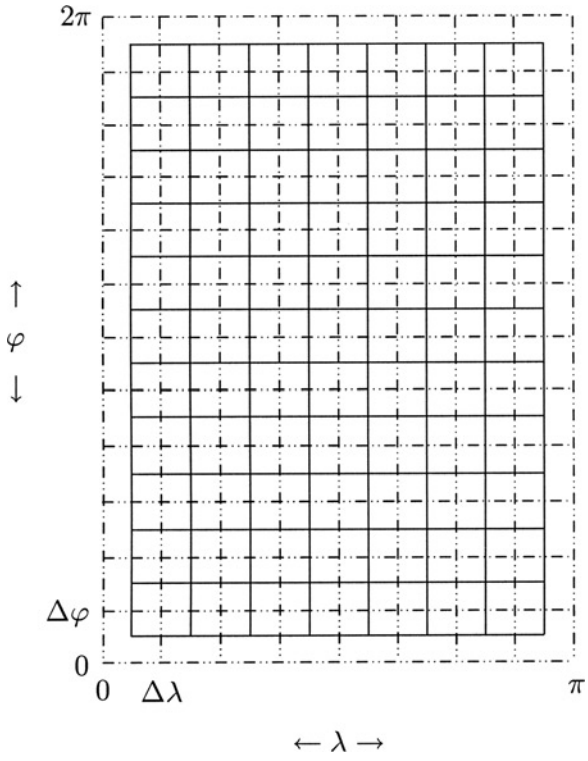

Figure 2.
The second coordinate map (dash-dot lines) and the corresponding grid covering (solid lines) for the sphere S

$$\frac{U_k^{n+1}-U_k^n}{\tau}+\frac{1}{2c_l}\left(\frac{\overline{u}_{k+1}U_{k+1}-\overline{u}_{k-1}U_{k-1}}{2\Delta\lambda}+\overline{u}_k\frac{U_{k+1}-U_{k-1}}{2\Delta\lambda}\right) = -\frac{g\overline{z}_k}{c_l}\frac{h_{k+1}-h_{k-1}}{2\Delta\lambda}, \tag{63}$$

$$\frac{V_k^{n+1}-V_k^n}{\tau}+\frac{1}{2c_l}\left(\frac{\overline{u}_{k+1}V_{k+1}-\overline{u}_{k-1}V_{k-1}}{2\Delta\lambda}+\overline{u}_k\frac{V_{k+1}-V_{k-1}}{2\Delta\lambda}\right)=0, \tag{64}$$

$$\frac{H_k^{n+1}-H_k^n}{\tau}+\frac{1}{c_l}\frac{\overline{z}_{k+1}U_{k+1}-\overline{z}_{k-1}U_{k-1}}{2\Delta\lambda}=0, \tag{65}$$

while in the direction φ we shall get:

$$\frac{U_l^{n+1}-U_l^n}{\tau}+\frac{1}{2c_l}\left(\frac{\overline{v}_{l+1}U_{l+1}\cos\varphi_{l+1}-\overline{v}_{l-1}U_{l-1}\cos\varphi_{l-1}}{2\Delta\varphi}+\overline{v}_l\cos\varphi_l\frac{U_{l+1}-U_{l-1}}{2\Delta\varphi}\right)=0, \tag{66}$$

$$\frac{V_l^{n+1}-V_l^n}{\tau}+\frac{1}{2c_l}\left(\frac{\overline{v}_{l+1}V_{l+1}\cos\varphi_{l+1}-\overline{v}_{l-1}V_{l-1}\cos\varphi_{l-1}}{2\Delta\varphi}+\overline{v}_l\cos\varphi_l\frac{V_{l+1}-V_{l-1}}{2\Delta\varphi}\right)=-\frac{g\overline{z}_l}{R}\frac{h_{l+1}-h_{l-1}}{2\Delta\varphi}, \tag{67}$$

$$\frac{H_l^{n+1}-H_l^n}{\tau}+\frac{1}{c_l}\frac{\overline{z}_{l+1}V_{l+1}\cos\varphi_{l+1}-\overline{z}_{l-1}V_{l-1}\cos\varphi_{l-1}}{2\Delta\varphi}=0. \tag{68}$$

Here $c_l=R\cos\varphi_l$. Analogously, schemes of other orders can easily be written. The rotation subproblem is:

$$\frac{U_{kl}^{n+1}-U_{kl}^n}{\tau}-\left(f_l+\frac{\overline{u}_{kl}}{R}\tan\varphi_l\right)V_{kl}=0, \tag{69}$$

$$\frac{V_{kl}^{n+1}-V_{kl}^n}{\tau}+\left(f_l+\frac{\overline{u}_{kl}}{R}\tan\varphi_l\right)U_{kl}=0, \tag{70}$$

and formulas similar to (61)-(62) can easily be obtained.

It is noteworthy that the use of two different maps (61)-(62) is possible exclusively due to the splitting. Thereby, if (54) holds, we keep the simple M-diagonal structure of the matrices, and hence the solution appears to be cheap from the computational standpoint. In this connection we emphasise that if one solves the complete 2D shallow-water system without splitting then the problem of complicating the matrix structure evidently arises.

6. Numerical results

Now we shall illustrate how the developed method works, simulating the behaviour of nonlinear soliton-like waves generated by a model topography. The schemes of the first four approximation orders in space will be tested. Because each finite difference scheme exactly conserves the mass and the total energy, but not the potential enstrophy, temporary behaviour of the latter is considered as an important integral characteristic of the schemes' quality in all the experiments. Besides, spatial structure of the solution at different time moments will be analysed in detail.

We took a simple set of the initial conditions $H(\lambda, \varphi, 0) = 3{,}000\ m$, $u(\lambda, \varphi, 0) = 0$, $v(\lambda, \varphi, 0) = 0$, and introduced a relief given by two mountains, whose heights did not exceed $1{,}000\ m$ (Figure 3). The larger mountain covers the area from $-50°$ to $+50°$ meridionally, locating at 250°-280° eastwards, which roughly corresponds to the American Cordillera including the mountains of North, Central and South America. The smaller mountain is located near 30°-50° northwards and 80°-100° eastwards simulating the Himalaya. Note that we did not keep the height ratio between the real mountains and the model ones. The grid spacings $\Delta\lambda$, $\Delta\varphi$ and τ were chosen such that the finite difference schemes were accurate and the matrices corresponding to each split system were diagonally dominant. The schemes were tested on the sequence of grids $12° \times 12°$, $6° \times 6°$, $3° \times 3°$ and $1.5° \times 1.5°$.

It is well-known that a numerical solution to the SWM obtained with a finite difference scheme of an odd approximation order in space contains either physical or computational modes. This depends on whether the advective terms are approximated correctly from the physical standpoint. On the other hand, schemes of even approximation orders simultaneously generate both physical and computational modes (Press *et al.*, 1992). To verify these facts, in Table I we

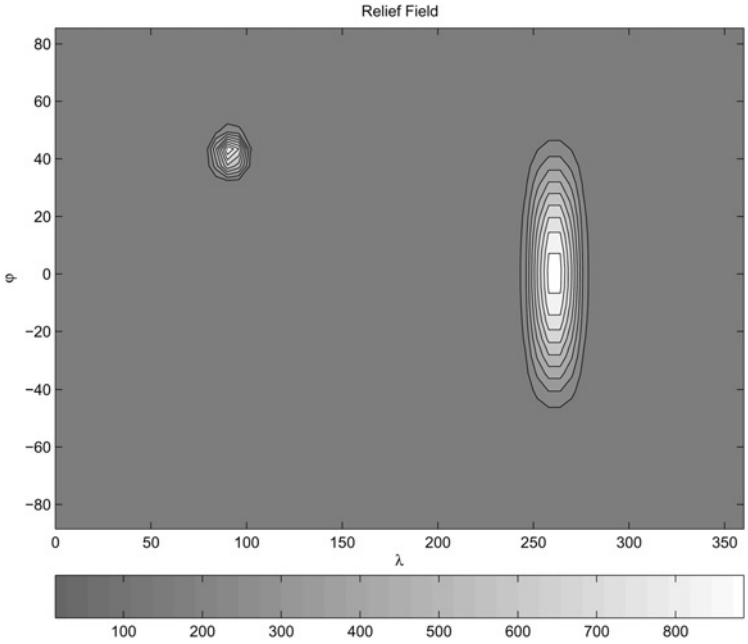

Note: Maximum height of the mountains is about 900 m

Figure 3.
Relief used in the numerical experiments

Grid	1st	2nd	1st-2nd	3th	4th	3rd-4th
$12° \times 12°$	1.129	0.396	0.326	1.091	0.212	0.151
$6° \times 6°$	1.661	0.130	0.102	1.287	0.102	0.081
$3° \times 3°$	>10	0.047	0.041	>10	0.051	0.046
$1.5° \times 1.5°$	>10	0.039	0.030	>10	0.046	0.038

Table I.
Maximum variation (in per cent) of the potential enstrophy for schemes of different approximation orders

summarise the maximum variation of the potential enstrophy obtained with the SWM schemes of the first four orders. So, in accordance with the theory, the purely odd-order schemes provided physically unreliable solutions, just because neither up-wind-like nor down-wind-like schemes are suitable for simulating such a complicated flow. The corresponding results are shown in Table I in the columns "1st" and "3rd". Unlike that, the even-order schemes approximated the solution in a suitable manner and provided reliable results: maximum variation of the potential enstrophy gets down while refining the grid (columns "2nd" and "4th" of the table).

In order to reduce the effect of computational modes generated by even-order schemes, we used 'conditional' computing. Namely, when computing in the direction λ, at each fixed φ_l we employed an odd-order up-wind scheme if all the $\overline{u}_k$'s were positive, an odd-order down-wind scheme if all the $\overline{u}_k$'s were negative, or the even-order scheme if there were the $\overline{u}_k$'s of both signs. Similarly we did in the direction φ checking each time the signs of the $\overline{v}_l$'s. Therefore we slightly improved the solution (compare columns "1st"-"2nd" vs "2nd" and "3rd"-"4th" vs "4th", respectively). Because of complexity of the flow the odd-order schemes were applied rather seldom, and so the improvement was not substantial. However, the more the directional is the flow, the more the essential accuracy improvement can be achieved while using odd-order schemes (Skiba and Filatov, 2007, 2008).

In Figure 4 we plot graphs of the potential enstrophy in time. As one may see, the variations are within narrow bands and very small – the quantity $\delta J(t) \equiv \max J(t) - \min J(t) / \min J(t) \cdot 100$ per cent does not exceed 0.05 per cent on fine ($3^\circ \times 3^\circ$ or better) grids (Table I).

We found out that the taken initial conditions generate a stable λ-periodic soliton-like solution $\vec{\eta} = (u, v, H)^{\mathrm{T}}$, whose depth field has two observable peaks. In Figure 5 we show the function $H(\lambda, \varphi, t)$ for several time moments. It can be seen that just in the beginning the larger mountain ("Cordillera") generates two solitary peaks (located at $\lambda \approx 210^\circ - 220^\circ$ and $\lambda \approx 300^\circ - 310^\circ$, respectively) propagating eastwards and westwards ($t = 0.2$). Because the first peak (travelling to the east) goes to the same direction that the sphere rotates, it keeps its form and magnitude almost unchanged during all the time of modelling. Unlike, the second peak propagates to the opposite direction, and all obstacles and waves it meets perturb its shape substantially. This is observed especially clear in Figure 6: one can see a strong local zonal flow (located at $\lambda = 290^\circ - 320^\circ$ at $t = 0.2$, and so on) that transports the first peak and a turbulent convergent divergent vortex (well observed at $\lambda = 220^\circ - 250^\circ$ at $t = 0.2$) which moves the second, weake peak. Note that the "Himalaya" mountain also produces wave solutions, which, however, have much smaller amplitudes compared to those generated by the larger mountain (nicely observed at $t = 0.2$).

From $t = 1.1$ to $t = 1.5$ we observe an interaction of the two peaks at $\lambda \approx 100^\circ - 110^\circ$. Again, the first peak remains almost unperturbed, whereas the second one changes its shape and loses in the amplitude (Figure 5, $t = 1.5$). In Figure 6 the same peaks interaction is shown as it is modelled by the velocity field.

In Figures 7 and 8 we show the propagation of the peaks over the "Cordillera" mountain. What is interesting here is that we can observe two different manners of propagation of the solitary waves over an obstacle. Indeed, the stronger peak goes over the 'Cordillera' without considerable changes both in the depth and velocity fields (Figures 7 and 8, $t = 2.0 - 2.4$). On the other hand, the weaker solitary wave, being

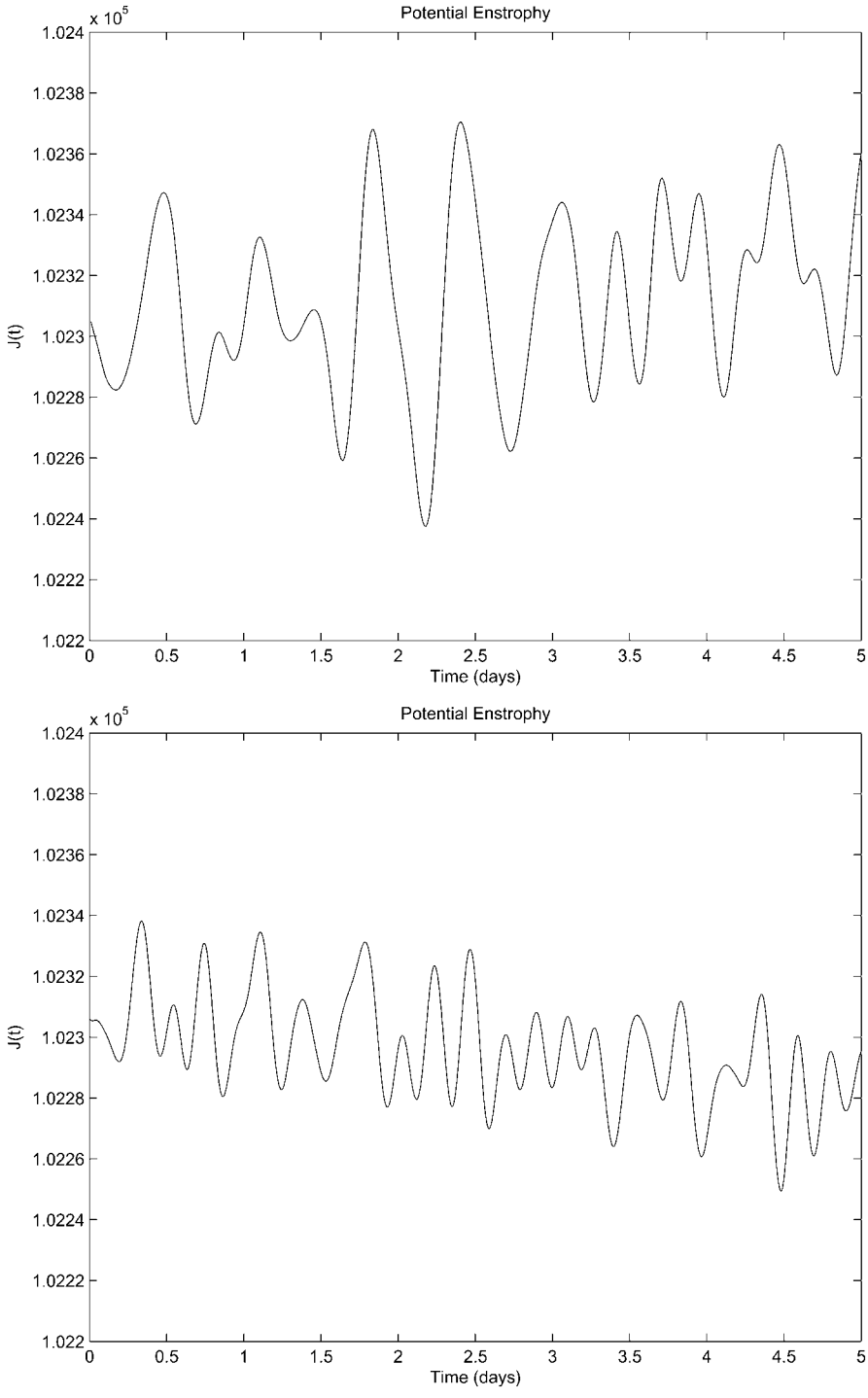

Figure 4.
Behaviour of the potential enstrophy $J(t)$ in time on the grid $3^\circ \times 3^\circ$, $\tau = 3.6$ min, second-order (top) and fourth-order (bottom) schemes

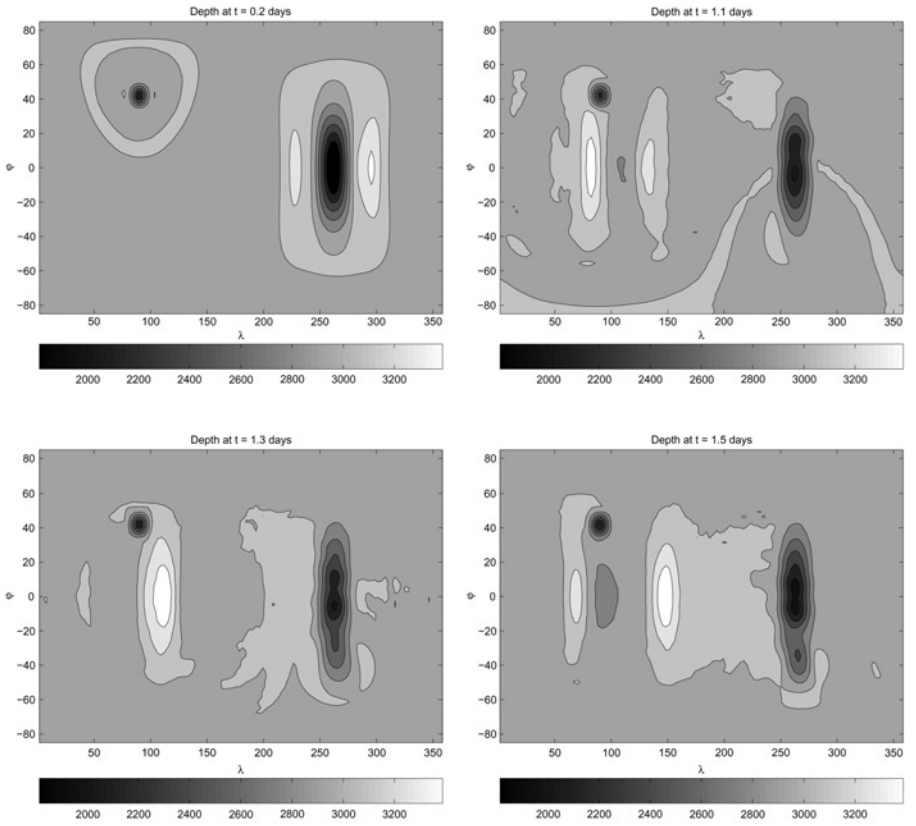

Figure 5.
Depth field

Note: Generation and subsequent interaction of two solitary peaks propagating in opposite directions

located at $t = 2.6$ between the "Cordillera" and the stronger peak, changes its velocity field essentially when passing the mountain at $t = 2.8$ (Figure 8).

In Figures 9 and 10 we show the solution for further time moments. While propagating, the peaks meet one another and interfere at $t = 3.7$. After the nonlinear interaction the waves continue propagating east- and westwards, which is clearer to observe in Figure 10 than in Figure 9. Comparing the solutions at $t = 1.3$ and $t = 3.7$, we find the full period of revolution over the sphere to be $\Delta T = 3.7 - 1.3 = 2.4$ days. At the same time, the gravitational waves revolution is known to be $\Delta T_{grav} = 2\pi R/\sqrt{gH} \approx 40 \cdot 10^6\,\mathrm{m}/171\,\mathrm{m/s} = 2.7$ days (Pedlosky, 1982; Vreugdenhil, 1994), and, following the theory of nonlinear waves propagation (Kundu, 1990), the time ΔT should be a little bit greater than ΔT_{grav}. The explanation for why ΔT happened to be less than ΔT_{grav} is the effect of nonlinear wave interaction. Indeed, say, in Figure 5 we see that the stronger peak, when interacting with the weaker one, passes from $\lambda \approx 80^\circ$ $(t = 1.1)$ to $\lambda \approx 150^\circ$ $(t = 1.5)$ for $t = 1.5 - 1.1 = 0.4$ days. Without the nonlinear interaction such a rapid translation would be impossible, since it requires the solitary wave velocity to be close to 225 m/s. The same is observed in Figure 7: here the stronger peak, due to the nonlinear interaction with the 'Cordillera'

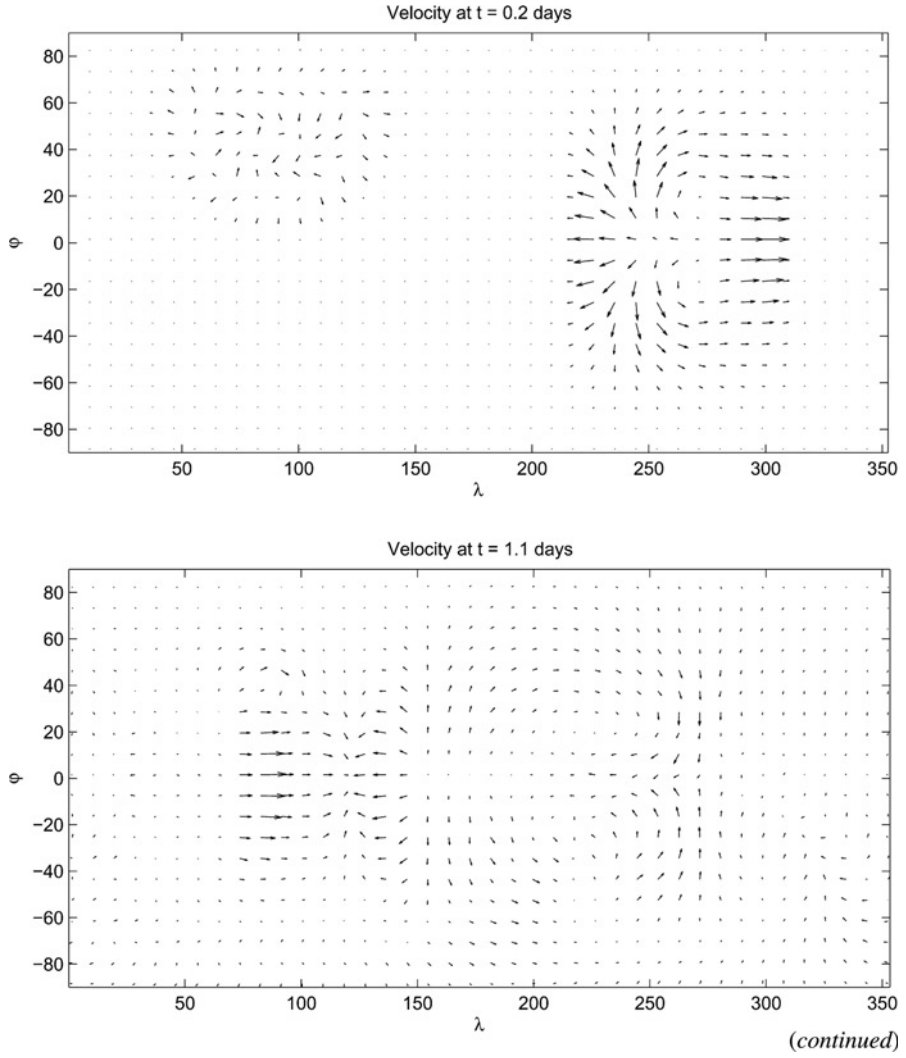

Figure 6.
Velocity field

mountain, passes from $\lambda \approx 230^\circ$ ($t = 2$) to $\lambda \approx 290^\circ$ ($t = 2.4$) for the same 0.4 days, which translation would only be possible at the peak's velocity about 193 m/s.

7. Conclusions

Conservative finite difference schemes of arbitrary approximation orders in space for shallow-water flows on a rotating sphere have been suggested. An essential advantage of the underlying method is that it produces fully discrete (both in time and in space) shallow-water schemes that exactly conserve the mass and the total energy and whose numerical implementation is computationally inexpensive.

Our approach is based on splitting of the SWM operator by coordinates and by physical processes. As a result, the solution to the original system of 2D partial differential equations reduces the solution to three simple problems containing either

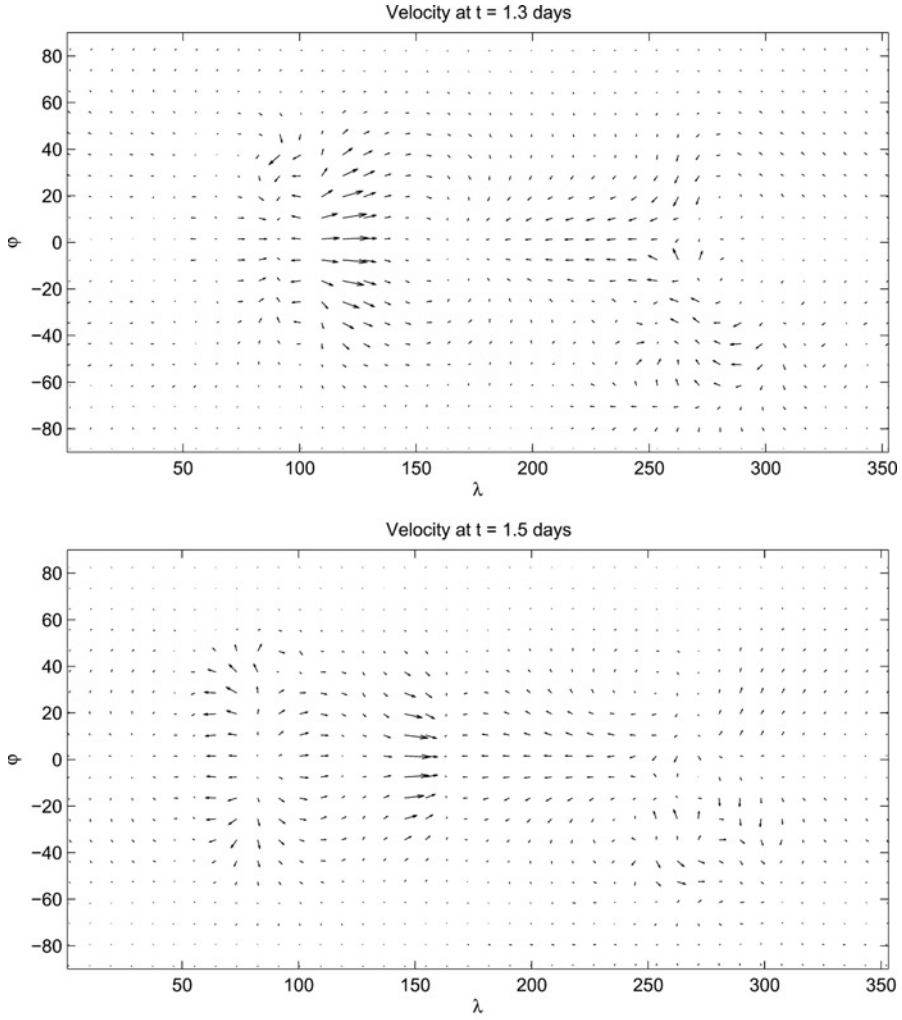

Figure 6.

Notes: Generation and subsequent interation of two solitary peaks propagating in opposite directions

1D partial differential equations or ordinary differential equations. In fact, an infinite family of such conservative schemes is proposed, which are either linear or nonlinear depending on the choice of certain parameters of the scheme.

On a doubly periodic manifold (for example, on a doubly periodic domain on the plane, or on a 2D torus) the method allows constructing conservative finite difference schemes of arbitrary approximation orders in space. Moreover, if the SWM is considered on the whole sphere then the method allows using the same numerical algorithms as for a doubly periodic manifold, providing with schemes of arbitrary approximation orders in the spherical geometry. The numerical SWM algorithms developed are computationally cheap, because each scheme is easily implemented by using band methods of linear algebra.

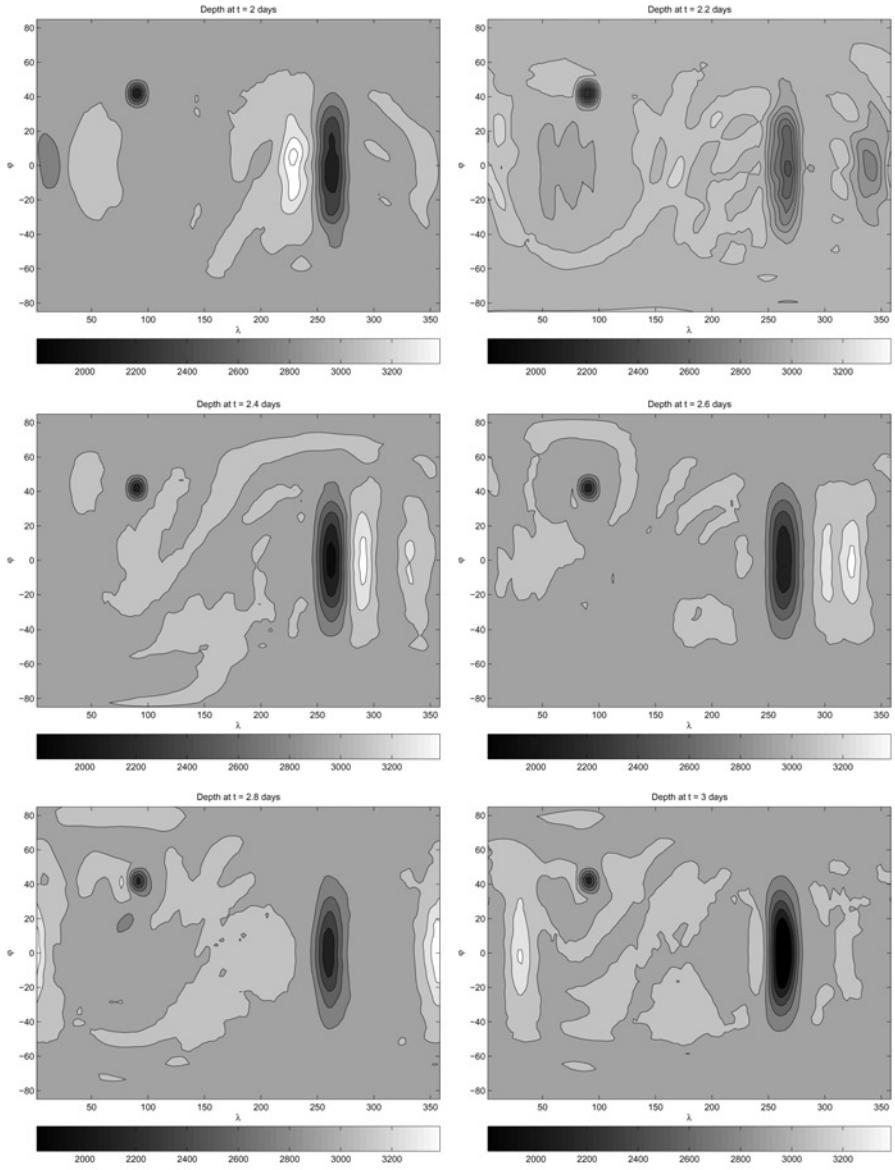

Note: Propagation of solitary waves over a mountain

Figure 7.
Depth field

The virtue of the finite difference schemes has been illustrated via the simulation of nonlinear soliton-like waves generated by a model topography. The numerical experiments included testing and comparison of the finite difference schemes of the first four orders on grids of different resolutions. The primary attention was given to the study of time–space structure of the numerical solutions. We stress that each finite difference scheme exactly conserves the mass and the total energy, but not

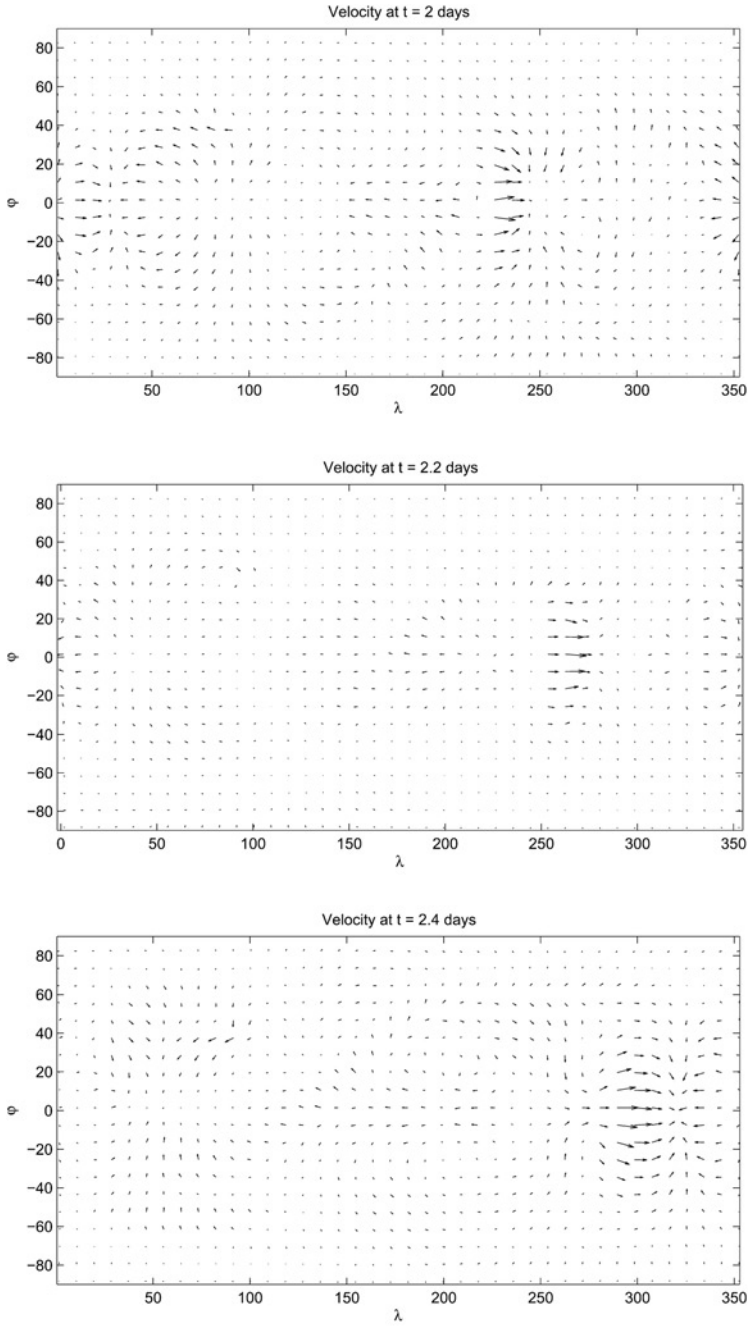

(*continued*)

Figure 8.
Velocity field

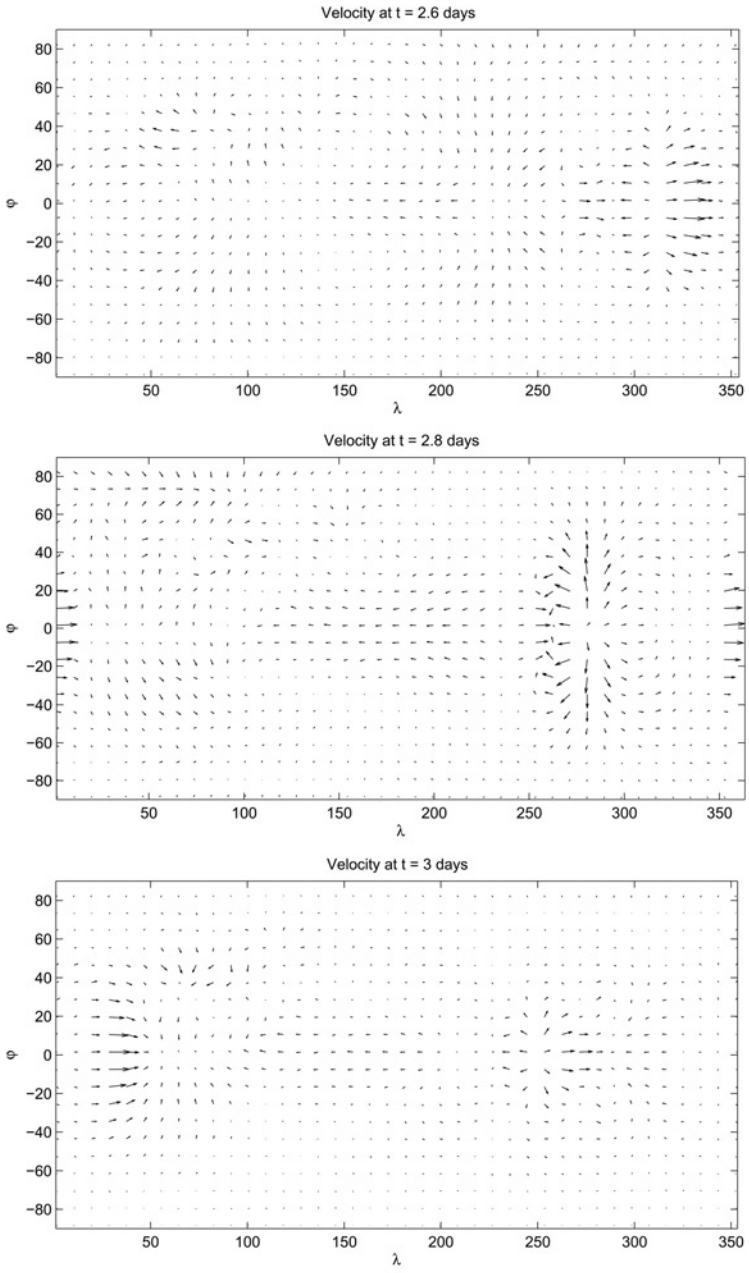

Note: Propagation of solitary waves over a mountain

Figure 8.

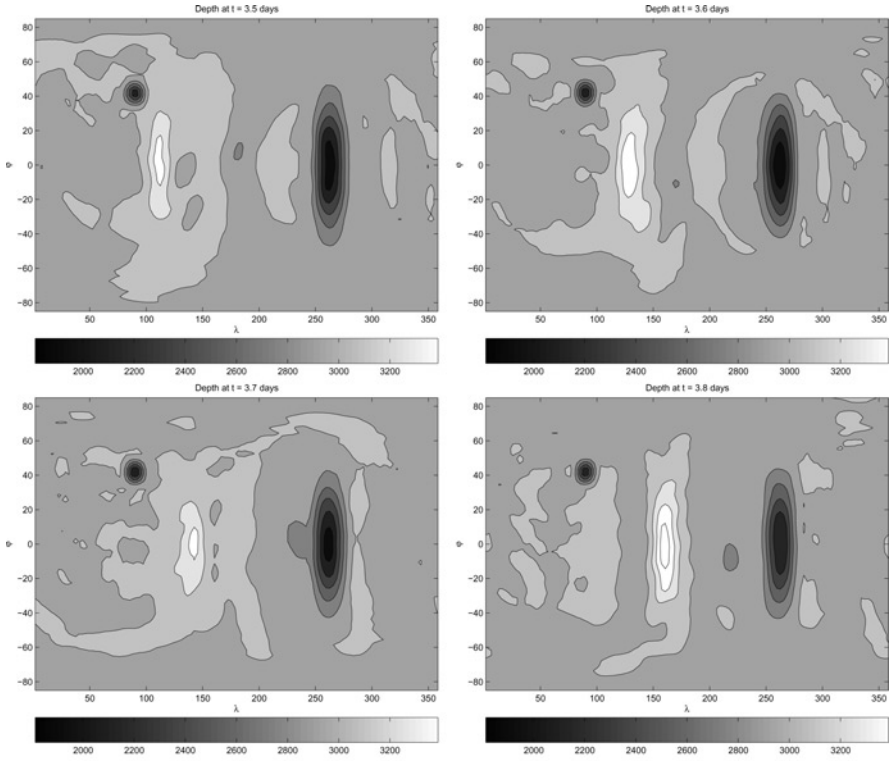

Figure 9.
Depth field

Note: Stability and periodicity of the solution

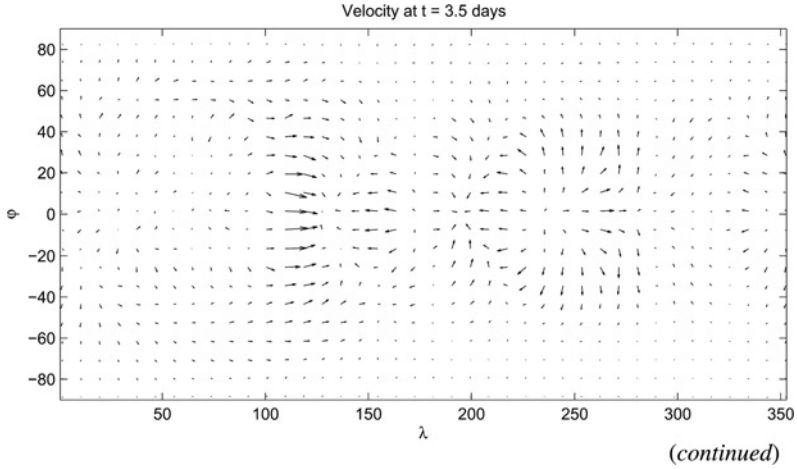

Figure 10.
Velocity field

(continued)

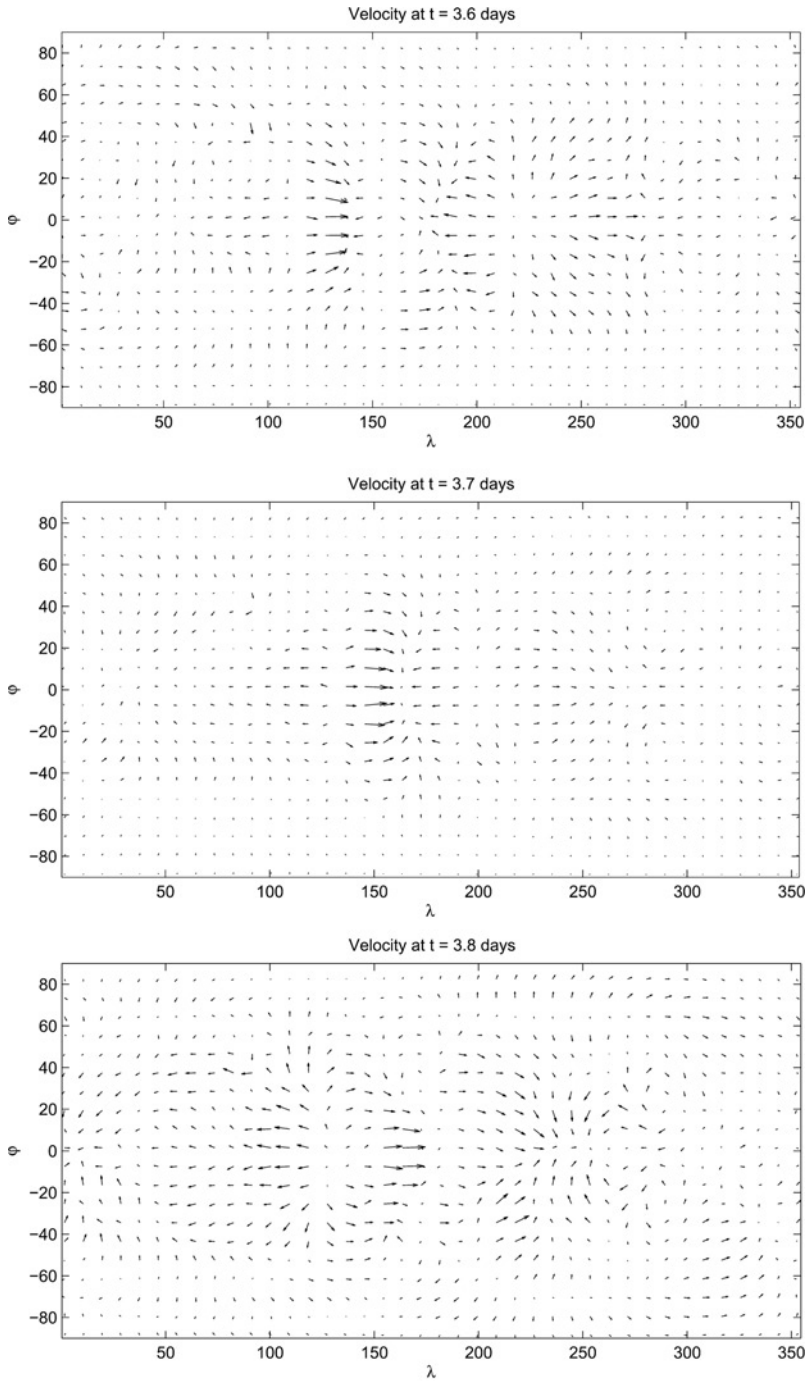

Note: Stability and periodicity of the solution

Figure 10.

the potential enstrophy. Since the potential enstrophy is one of the basic invariants of the shallow-water motion, temporary behaviour of the potential enstrophy was considered as an important integral characteristic of the schemes' quality in all the experiments. The even-order schemes, taken alone or coupled with the "conditional" computing, proved to be good for modelling complicated flows; the odd-order schemes should only be used for simulating strictly one-way streams, such as zonal flows or similar.

References

Arakawa, A. and Lamb, V.R. (1981), "A potential enstrophy and energy conserving scheme for the shallow-water equation", *Monthly Weather Review*, Vol. 109, pp. 18-36.

D'yakonov, E.G. (1964), "Difference schemes of the second order with a splittable operator for parabolic equations without mixed partial derivatives", *Journal of Computational Mathematics and Mathematical Physics*, Vol. 4, pp. 935-41.

D'yakonov, E.G. (1972), *Difference Methods of Solution to Boundary Value Problems. Vol. 2, Non-Stationary Problems*, Moscow State University Press, Moscow.

Kim, V.F. (1984), "Numerical analysis of some conservative schemes for barotropic atmosphere", *Russian Meteorology & Hydrology*, Vol. 6, pp. 251-61.

Korn, G.A. and Korn, T.M. (1968), *Mathematical Handbook for Scientists and Engineers*. McGraw-Hill, New York, NY.

Kundu, P.K. (1990), *Fluid Mechanics*, Academic Press, San Diego, CA

Marchuk, G.I. (1982), *Methods of Computational Mathematics*, Springer-Verlag, Berlin.

Morton, K. and Mayers, D. (1994), *Numerical Solution of Partial Differential Equations*, Cambridge University Press, Cambridge.

Pedlosky, J. (1982), *Geophysical Fluid Dynamics*, Springer-Verlag, Berlin.

Press, W.H. *et al.* (1992), *Numerical Recipes in C. The Art of Scientific Computing*, Cambridge University Press, Cambridge.

Ringler, T.D. and Randall, D.A. (2002), "A potential enstrophy and energy conserving numerical scheme for solution of the shallow-water equations on a geodesic grid", *Monthly Weather Review*, Vol. 130, pp. 1397-410.

Sadourny, R. (1975), "The dynamics of finite difference models of the shallow-water equations", *Journal of the Atmospheric Sciences*, Vol. 32, pp. 680-9.

Salmon, R. (2004), "Poisson-bracket approach to the construction of energy- and potential-enstrophy-conserving algorithms for the shallow-water equations", *Journal of the Atmospheric Sciences*, Vol. 61, pp. 2016-36.

Samarskii, A.A. and Popov, Yu.P. (1969), "Completely conservative difference schemes", *Journal of Computational Mathematics and Mathematical Physics*, Vol. 9, pp. 953-8.

Shokin, Yu.I. (1988), "Completely conservative difference schemes", in de Vahl Devis, G. and Fletcher, G. (Eds), *Computational Fluid Dynamics*, Elsevier, Amsterdam, pp. 135-55.

Skiba, Yu.N. (1995), "Finite difference mass and total energy conserving schemes for shallow-water equations", *Russian Meteorology & Hydrology*, Vol. 2, pp. 35-43.

Skiba, Yu.N. and Filatov, D.M. (2007), "On splitting-based mass and total energy conserving arbitrary order shallow-water schemes", *Numerical Methods for PDEs*, Vol. 23, pp. 534-52.

Skiba, Yu.N. and Filatov, D.M. (2008), "Conservative arbitrary order finite difference schemes for shallow-water flows", *Journal of Computational and Applied Mathematics*, Vol. 218, pp. 579-91.

Takano, K. and Wurtele, M.G. (1982), "A four-order energy and potential enstrophy conserving difference scheme", The US Air Force Geophysics Laboratory, Technical Report AFGL-TR-82-0205 Ch. 2, Hanscomb AFB, MA. p. 85

Vreugdenhil, C.B. (1994), *Numerical Methods for Shallow-Water Flow*, Kluwer Academic, Dordrecht.

Williamson, D.L. (1979), "Difference approximations of flow equations on the sphere", in *Numerical Methods Used in Atmospherical Models*, GARP Publ. Series, No 17, Vol. II, pp. 51-120, JOC, WMO, Geneva.

Yanenko, N.N. (1971), *The Method of Fractional Steps: Solution to Problems of Mathematical Physics in Several Variables*, Springer-Verlag, Berlin.

Further reading

Jakob-Chien, R. *et al.* (1995), "Spectral transform solutions to the shallow water test set", *Journal of Computational Physics*, Vol. 119, pp. 164-87.

Williamson, D.L. *et al.* (1992), "A standard test set for numerical approximations to the shallow water equations in spherical geometry", *Journal of Computational Physics*, Vol. 102, pp. 211-24.

Corresponding author

Denis M. Filatov can be contacted at: denisfilatov@gmail.com